Hindawi
Scientific Programming
Volume 2021, Article ID 4100856, 8 pages
https://doi.org/10.1155/2021/4100856

Research Article

Classification Algorithm-Based CT Imaging in Diagnosis of Acute Respiratory Distress Syndrome and Analysis of Pathogenic Factors

Liang Chen and Qiong Li

Department of Critical Care Medicine, The First People's Hospital of Chenzhou, Chenzhou 423000, Hunan, China

Correspondence should be addressed to Qiong Li; 141008140102@st.sdju.edu.cn

Received 31 August 2021; Revised 14 October 2021; Accepted 15 October 2021; Published 8 November 2021

Academic Editor: Gustavo Ramirez

The study focused on the application value of classification algorithms in processing CT images of acute respiratory distress syndrome (ARDS) and aimed to analyze the pathogenic factors of ARDS. A total of 60 ARDS patients in hospital were selected, and they were divided into ARDS group (38 cases) and non-ARDS group (22 cases) as per diagnostic criteria. There was no significant difference in general data between the two groups ($P > 0.05$). The FWAC algorithm was introduced into CT imaging to classify the image data more accurately. The two groups were compared for the left ventricular ejection fraction (LVEF), oxygenation index PaO_2/FiO_2 (P/F), Acute Physiology and Chronic Health Evaluation (APACHE II) scores, pH, and PaO_2. The results showed that the PaO_2, P/F, and APACHE II scores of the two groups were not statistically significant ($P > 0.05$). The P/F of the ARDS group was 136.12, and that of the non-ARDS group was 143.04; the APACHE II score of the ARDS group was 40.1, and that of the non-ARDS group was 62.3, showing no significant difference ($P > 0.05$); the LVEF of the ARDS group was 58.14, and that of the non-ARDS group was 46.26, showing statistically significant differences ($P > 0.05$). When the minimum support was 0.3 and the minimum confidence was 0.5, the value of Recurrence was 0.7082 and the value of Diagnosis was 0.968. The rules generated by the FWAC algorithm can accurately predict the category and were consistent with the expected results. The accuracy of this algorithm was as high as 98.7%, which was significantly higher than that of the conventional CT imaging (88.4%). The rules generated by FWAC were more accurate, assisting doctors in the prevention and diagnosis of ARDS disease. Premature delivery and asphyxia are high-risk factors of ARDS. In conclusion, the FWAC algorithm has a good classification ability of the CT images of ARDS and demonstrates high accuracy.

1. Introduction

The acute respiratory distress syndrome (ARDS) is a common type of acute respiratory failure arising from damage to the alveoli and capillary membranes and increased capillary permeability, and the fatality rate of ARDS is as high as 40%–70% [1]. The common primary diseases of ARDS include sepsis, pneumonia, and severe trauma. As for the pathological basis of this disease, many kinds of inflammatory cells mediate inflammatory reactions in the lungs and will lead to type II alveolar epithelial cell injury, when the inflammation is out of control and then pulmonary microvascular permeability will increase, leading to pulmonary interstitial edema [2]. ARDS is a pulmonary vascular tissue disorder. For patients suffering from ARDS, the water content of the lung increases and the compliance decreases, which eventually leads to respiratory distress and hypoxemia. The annual mortality rate of ARDS is gradually increasing, and severe trauma and pneumonia will cause respiratory distress. Hence, the research on risk factors related to ARDS and its epidemiology is important [3]. ARDS has complex pathogenesis, acute onset, and rapid progression and is difficult to treat. Furthermore, it has poor prognosis and high mortality. The effect of drugs on ARDS is not ideal, and the key to treating ARDS is usually early diagnosis and treatment [4].

Computed tomography (CT) is an important basis for the diagnosis of lung imaging [5]. Pulmonary vascular CT

imaging can reconstruct three-dimensional images. As a diagnostic method of ARDS, CT can clearly show the pulmonary blood vessels. Multislice spiral CT optimizes the image acquisition and analysis technology [6, 7]. CT imaging technology has been widely used in medical, industrial, and other fields. In the actual CT scanning process, due to the limited size of the detector or the large size of the object, the projection data on the detector is truncated and the reconstructed CT image can only reflect part of the object information. The high-resolution CT image can show the changes in the lungs [8]. Research results show that high-resolution CT can detect some characteristic changes in septic lung segments and subpulmonary embolism, such as "wedge-shaped shadow" and "connected vascular shadow" [9]. The CT vascular perfusion imaging can quantitatively analyze the blood perfusion of the local tissue, which can reflect the changes in physiological functions in time. With the continuous development of microelectronics and computer technology, CT is also constantly updated and improved. Incorporating classification algorithms into CT imaging provides a new method to accurately diagnose and classify diseases.

The use of high-tech medical equipment has increased the amount of medical data, and extracting valuable data from complex medical data can provide an effective reference for the analysis of disease risk factors [10]. Currently, the classification algorithms include traditional random forests, neural networks, and support vectors. They have classification accuracy, but it is not easy to find characteristics that affect the disease. The association classification algorithm can dig out the effective features related to the disease, and most of the association classification counting algorithms applies association rules in the classification to strengthen the classification and the weighted association classification algorithm generates more accurate rules for the characteristics of harmonic mean. The association classification algorithm can register the corresponding category information in each node and directly mine the class association rules with minimum support and minimum confidence. When scanning the database, there is no need to repeat the established conditions, which reduces the memory consumption and effectively improves the operation efficiency. The essence of classical association classification algorithm is to adopt confidence degree, support degree, and rule item so that it can consider both confidence degree and support degree comprehensively [11]. In this study, an association classification algorithm was used and pruned by statistical measurement technology to obtain more accurate association rules and improve the accuracy of the association classifier. It was trained using the ARDS disease data set in the machine learning database, to obtain more accurate treatment and diagnosis results, expected to provide a reference for the treatment of ARDS.

2. Materials and Methods

2.1. Characteristics of Medical Data. Medical data are generated when a patient is diagnosed and treated in hospital. The information of patients, such as image data, medical orders, and prescription information, is special and diverse, and there is a large amount of imaging data obtained through CT and color Doppler ultrasound.

Data mining is a technology that extracts knowledge or patterns from data so that some hidden potential information is mined. Using relevant algorithms to obtain disease information from massive medical data can assist physicians in diagnosis and treatment. The steps of medical data mining are shown in Figure 1.

2.2. Steps of Association Classification Algorithm. Compared with the neural network algorithm, the association classification algorithm has good classification accuracy, can generate more understandable rules, and can also find rare rules. The association classification algorithm mainly includes three stages: the generation of the classification rules, the construction of the rules, and the prediction. The specific flow chart is shown in Figure 2. In the first step, frequent item sets can be generated according to related algorithms such as FP-Growth and Eclat and then based on the minimum confidence threshold and minimum support, the rules are pruned, including χ^2 tests, database coverage, and classification prediction.

2.3. Association Classification Algorithm. Association classification mainly uses association mining algorithms to classify data sets according to frequent rules, construct classifiers according to classification association rules, and finally predict a new data set classification. Association rule technology is mainly used to discover and classify the associations between various attributes in the database and then predict the category labels.

Suppose there is a data set of M and the training objects are $abcde$ of attribute 1 ($B1$), attribute 2 ($B2$), attribute 3 ($B3$)...; in this problem, the association rules apply to the classification process. If $Bt_1 \longrightarrow D1$ belongs to a rule, then D_1 is a class attribute. (Bt_1, Bt_2, Bt_3, ..., Bt_n) indicates that the training set M has N different attributes, and D indicates a list of categories. Attributes include classification attributes and continuous attributes. Continuous attributes need to be discretized using a certain discretization method, and the categorical attributes are assigned a set of positive integers corresponding to the categorical attribute values one to one. The training object in M can be described as a combination of attribute D_i and Bt_1.

If D_i represents a class label, an itemset rule f [itemset, D_i] and the training object b [($B1$, $v1$) ($B2$, $v1$), D_i] have itemset rules. Then, for b [($B1$, $v1$) ($B2$, $v1$)], actoccr = 3. The number of rows matching rule f in M is the supporting technology of project rule f, $f \in D_i$, and then, the support counting equation is as follows:

$$\text{suppcount} = f \cup D_i. \tag{1}$$

If the item set rule $f \geq$ the minimum support threshold, then there is

$$\frac{\text{suppcount}(f)}{|M|) \geq \min \sup p}. \tag{2}$$

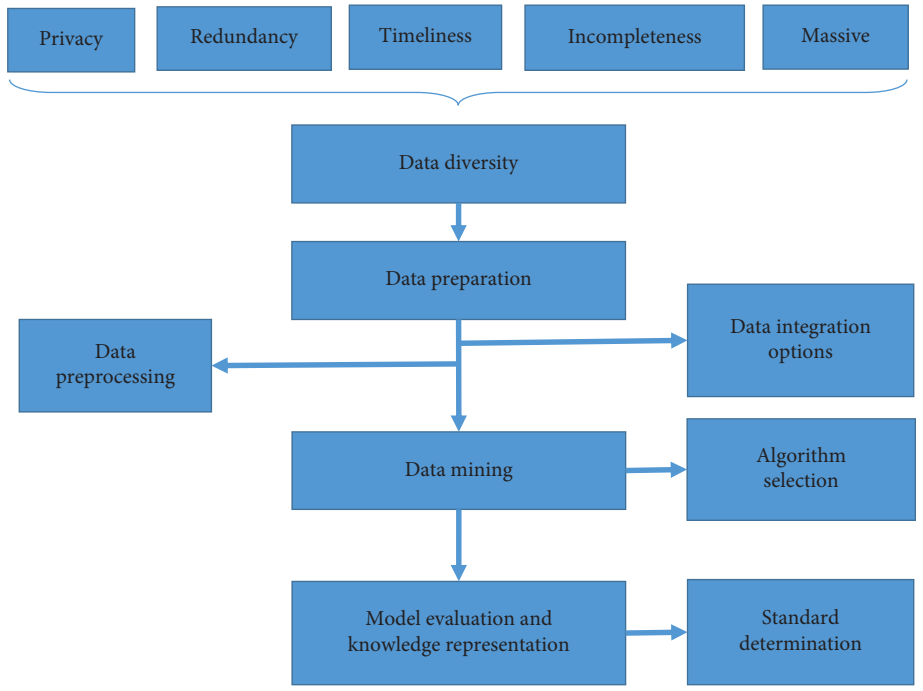

Figure 1: Data mining flow chart.

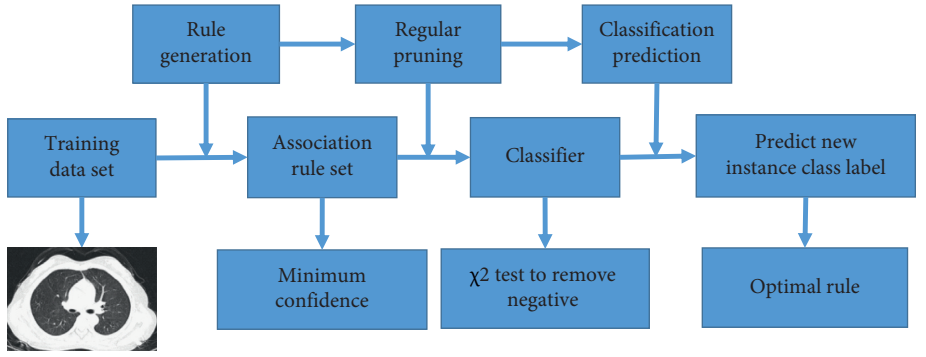

Figure 2: Flow chart of the associated classification algorithm.

$|M|$ represents the number of instances in M, and then, the support is calculated as follows:

$$\text{support} = \frac{\text{suppcount}(f)}{|M|}. \tag{3}$$

If the number of training objects in the data set is equal to 5, the suppcount of the itemset rule $[(B1, v1)\ (B2, v1), D_i]$ is equal to 2. According to the support equation, we will obtain the following equation:

$$\text{support} = \frac{2}{5} = 0.4. \tag{4}$$

In the case of the itemset rule $f \geq$ the minimum confidence threshold, that is,

$$\frac{\text{suppcount}(f)}{\text{actoccr}(f)) \geq \min \text{conf}}, \tag{5}$$

then the confidence level is expressed as follows:

$$\text{confidence} = \frac{\text{suppcount}(f)}{\text{actoccr}(f)}. \tag{6}$$

For the itemset $[(B1, v1)\ (B2, v1), D_i]$, there is

$$\begin{aligned} \text{suppcount} &= 2, \\ \text{actoccr} &= 3. \end{aligned} \tag{7}$$

Then, there is

$$\text{confidence} = \frac{2}{3}. \tag{8}$$

The classification association rule means that there is a set of frequent rules whose confidence is greater than or equal to the specified minimum confidence threshold. A frequent itemset rule can be regarded as the itemset rule f that meets the minimum support threshold.

Association classification algorithms have high accuracy. In the field of data mining, researchers can use classification

algorithms to find cases of rare diseases. Traditional classification algorithms directly filter out rare cases, and as a result, these rules cannot be mined. The association classification algorithm can overcome these shortcomings and generate more understandable rules.

2.4. Weighted Association Classification Algorithm. The association classification algorithm generates association rules. On this basis, a feature weighted association classification (FWAC) algorithm based on statistical harmonic average is used. The algorithm uses a weighted model instead of traditional association rules to mine the confidence structure. Figure 3 shows the three stages of FWAC, which are rule generation, rule construction, and data prediction. The generation of rules applies to the training set and the minimum support; the rule pruning is the construction of the minimum confidence; finally, a test set of predictions is obtained.

As for the process of rule generation, first, the training set (minimum support, N) is generated, $Y' = \Psi$ and $K = 1$, while $(Yk - 1 = \Psi)$; Y_k is the generated candidate k-item set f:

$$\begin{aligned} \text{support}(f) &= \frac{\text{suppcount}(f)}{n}, \\ \text{weight}(f) &= \frac{\text{weight}(\text{item}) + \cdots + \text{weight}(\text{item})}{k}, \\ \text{weight support}(f) &= \text{weight}(f) \times \text{support}(f). \end{aligned} \tag{9}$$

If weighted support $(f) \geq$ minimum support, $Y' = Y' + f$. If not, return to Y'.

2.5. General Information. The patients complaining of dyspnea admitted to hospital from January 2018 to June 2019 were selected as research subjects. All patients had the lung CT examination and chest X-ray examination within 24 hours after admission. Inclusion criteria were as follows: (I) patients without acute viral or bacterial infection; (II) patients having risk factors for ARDS: pneumonia, foreign body inhalation, extensive trauma, extrapulmonary sepsis; (III) patients with no immune system disease and no infectious disease; and (IV) patients with new respiratory symptoms or aggravation of existing respiratory symptoms within 7 days, shortness of breath, intractable and progressive hypoxemia, groaning, and nasal agitation. Exclusion criteria were as follows: (I) people with incomplete clinical data; (II) people who did not voluntarily participate in this research; (III) people with heart, liver, and kidney dysfunction; and (IV) people not cooperating in the CT examination. The difference was not statistically significant in the general data of patients ($P > 0.05$), and the general information was comparable. This study had been approved by the ethics committee of the hospital.

The gold standard for the diagnosis of ARDS: (I) children with related lung diseases during the perinatal period were excluded; (II) patients with symptoms of hypoxemia and changes in lung X-rays within 7 days; (III) patients with respiratory failure not arising from cardiac failure or excessive fluid overload; (IV) patients with pulmonary solid lesions consistent with the exudative changes in lung imaging; (V) during invasive mechanical ventilation, $5 \leq \text{OSI} < 7.5$ or $4 \leq \text{OI} \leq 8$ was diagnosed as mild ARDS, $8 \leq \text{OSI} < 16$ or $7.5 \leq \text{OI} \leq 12.3$ was diagnosed as moderate ARDS, and $\text{OI} \geq 16$ or $\text{OSI} \geq 12.3$ was diagnosed as severe ARDS; and (VI) during noninvasive mechanical ventilation, under CPAP ≥ 5 cm H_2O or full-face mask positive pressure ventilation, P/F ≤ 300.

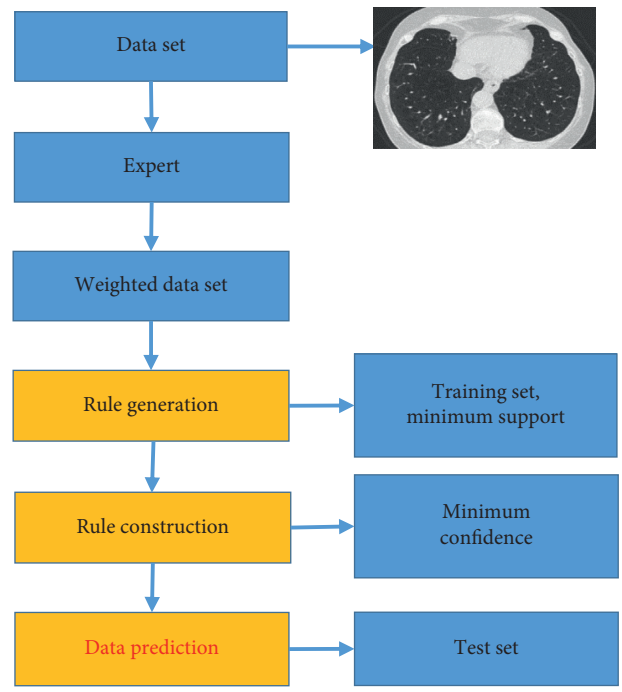

Figure 3: The FWAC algorithm.

2.6. CT Scan. In this study, patients were examined with Siemens Somatom definition DSCT (Germany). Before the scan, the examination procedure was explained in detail to the patient. The patient was in the supine position, and the second generation of Siemens was used for scanning. Tube current parameters were adjusted according to the weight, the machine automatically gave pitch, and the periodic exposure was fully automatic. 120 or 140 KV was for body mass > 90 kg, 100 or 120 KV was for 60 kg < body mass ≤ 90 kg, and 80 or 100 KV was for body mass ≤ 60 kg. At 165 mA or 140 mA, the rotation speed was 0.28 s/circle and the collimation was 64 × 0.6 mm; that is, each circle was 38.4 mm in length and the time resolution was 75 ms. To use the ECG-gated spiral scanning technology, the layer thickness was set to 0.6 mm, the layer distance was 0.75 mm, and the flow rate was 0.12 mL/s/kg using the MEDRED double-barrel high-pressure syringe. It was injected through the veins of the lower limbs, and the injection time was 20 seconds. The normal saline was injected at the same flow rate, and the maintenance time was 10 seconds. The scanning range was accurately located. The CT images of the best time sequence were selected and sent to the workstation

Syngo via VB10 B for image processing. All the images were evaluated by three chief physicians with more than 5 years of experience in the CT room using the double-blind method. When the opinions were inconsistent, the reconstructed images were evaluated again until the opinions were consistent.

2.7. Observation Indicators. The normal range of left ventricular ejection fraction (LVEF) is 50%–70%, and a mild reduction means that LVEF is 40%–50%; moderate reduction means that the LVEF is between 30% and 40%; and moderate reduction means LVEF <30%.

PaO_2/FiO_2 (P/F) is the oxygenation index, namely, the ratio of the arterial blood oxygen partial pressure to the inhaled oxygen concentration. Normally, it is between 400 and 500 mmHg. The oxygenation index is used clinically to reflect the oxygenation status of the body. The oxygenation index <300 mmHg indicates the lung respiratory function obstacle.

The Acute Physiology and Chronic Health Evaluation (APACHE II) is a comprehensive method to evaluate the severity of a patient's condition and predict the prognosis. It mainly includes three parts, acute physiology score, age score, and chronic health score. It is mainly used to classify and predict the prognosis of the patient's condition and to make a quantitative evaluation of the patient's condition.

2.8. Statistical Analysis. All data were processed using SPASS 21.0. The measurement data were expressed as $\overline{x} \pm s$, and the T-test was used. The count data were expressed as (n, %), and $P > 0.05$ indicated that there was a statistical difference. The factor analysis adopted multiple stepwise regression analyses.

3. Results

3.1. Comparison of General Information. Figure 4 shows the general data of the patients. The ARDS group (38) had 23 males and 10 females. In the non-ARDS group (22 cases), there were 10 males and 12 females. In the ARDS group, there were 7 cases of severe pneumonia, 9 cases of aspiration pneumonia, 6 cases of sepsis, and 4 cases of chronic lung disease. In the non-ARDS group, there were 5 cases of severe pneumonia, 6 cases of aspiration pneumonia, 4 cases of sepsis, and 3 cases of chronic lung disease. There was no statistical difference between the two groups of patients ($P > 0.05$).

3.2. Accuracy Comparison of Classification Algorithms. Figure 5 shows the CT images of the lung. Multiple filling defects can be seen in the main pulmonary artery and both inferior pulmonary artery branches. Figure 5(a) shows multiple filling defects in the right pulmonary artery, and a grade 3/6 systolic blowing murmur can be heard in the pulmonary artery area, which was not conducted to the apex of the heart. Figure 5(b) shows multiple filling defects in the left pulmonary artery. It was lobulated, projecting toward

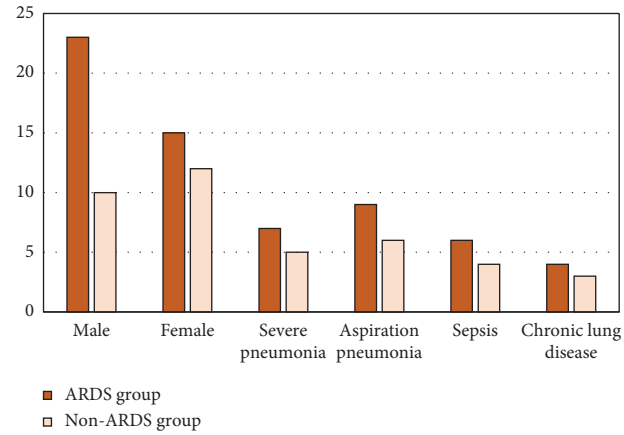

Figure 4: General information of the two groups of patients.

the proximal pulmonary artery like a bullet; it can almost be seen that it occupied the entire lumen and extended down to the sub-segment of the pulmonary artery, and the wall was not smooth. Figure 5(c) shows the density of ground glass under the oblique fissure of the middle lobe of the lung, and the subpleural exudative lesions of the lower lobe of the lung. In Figure 5(d), it was noted that one or both sides of the lung were spotted and fuzzy, that the lung texture was thickened, and that the edge of the consolidation shadow was blurred by the pleural shadow. The blue box in the figure marked the location of the lesion.

Then, the conventional CT and the association classification algorithm-based CT were compared for accuracy and the results are shown in Figure 6. The accuracy of conventional CT was 88.4%, and the accuracy of the association classification algorithm-based CT was 98.7%. The accuracy of the association classification algorithm-based CT was significantly higher than that of the conventional CT ($P > 0.05$).

3.3. Running Results of the FWAC Algorithm. The data set of ARDS patients was used to verify the performance of the FWAC algorithm, three different minimum support degrees were selected, and the minimum confidence degrees were all 0.5. As shown in Figure 7, when the minimum support was 0.2 and the minimum confidence was 0.5, the value of Recurrence was 0.7361 and the value of Diagnosis was 0.964; when the minimum support was 0.1 and the minimum confidence was 0.5, the value of Recurrence was 0.6972 and the value of Diagnosis was 0.971; when the minimum support was 0.3 and the minimum confidence was 0.5, the value of Recurrence was 0.7082 and the value of Diagnosis was 0.968. The rules generated by the FWAC algorithm can accurately predict the category and were consistent with the expected results.

3.4. Comparison of Measurement Data. Figure 8(a) shows that the P/F in the two groups was not statistically different ($P > 0.05$) but the difference in LVEF between the two groups was statistically significant ($P < 0.05$). Figure 8(b) shows the pH and PaO_2 of the two groups, and there was no

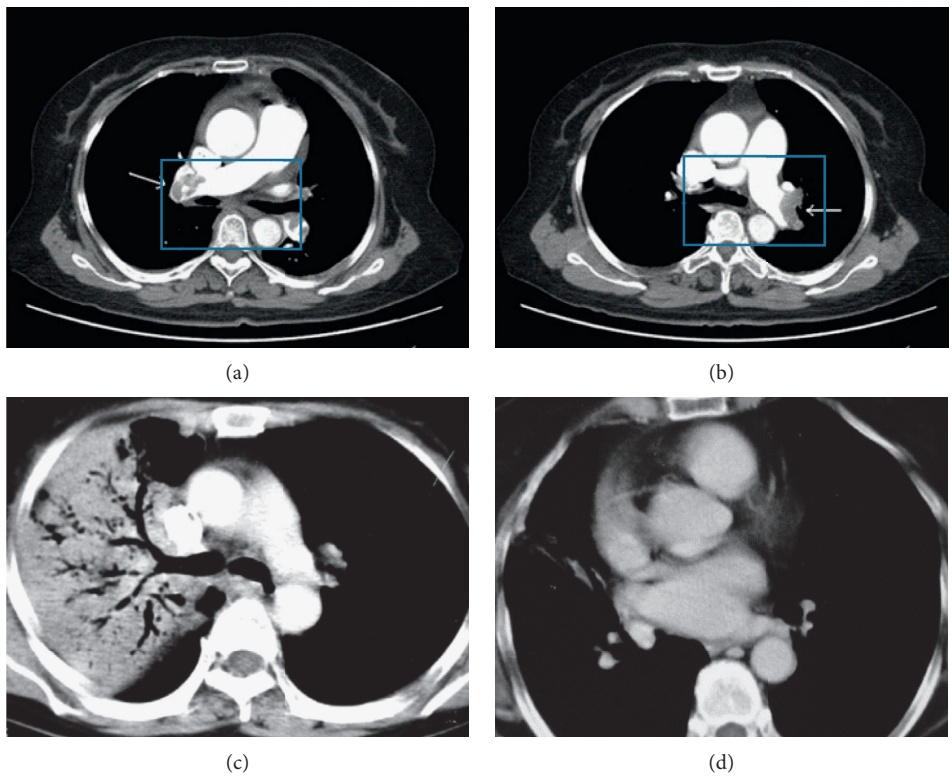

Figure 5: CT images. (a) Multiple filling defects in the right pulmonary artery; (b) multiple filling defects in the left pulmonary artery; (c) density of ground glass under the oblique fissure and subpleural exudative lesions; (d) spotted and fuzzy lung with thickened texture and blurred consolidation shadow.

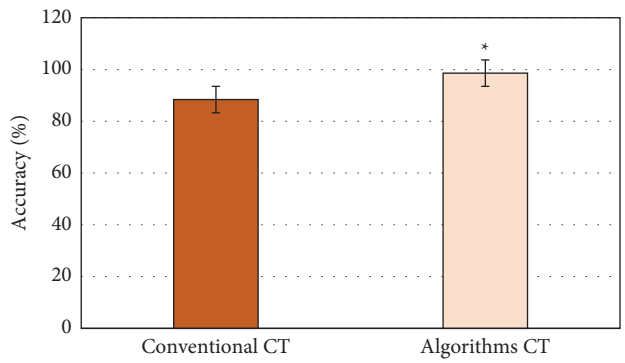

Figure 6: Accuracy comparison results. (*The difference was statistically significant).

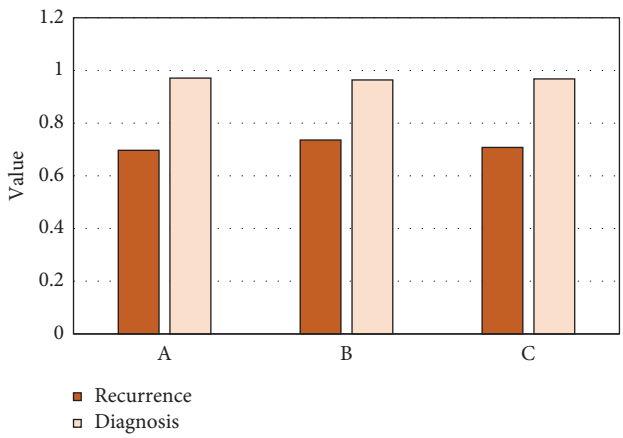

Figure 7: Performance of the FWAC algorithm. (a) Support = 0.1, confidence = 0.5; (b) support = 0.2, confidence = 0.5; (c) support = 0.3, confidence = 0.5.

significant difference between the two groups in pH and PaO_2 ($P > 0.05$).

3.5. Comparison of APACHE II Scores between the Two Groups. Figure 9 shows the APACHE II scores of the two groups. It was noted that the APACHE II score in the ARDS group was lower than that in the non-ARDS group and the difference was statistically significant ($P < 0.05$).

3.6. ARDS-Related Factor Analysis. The logistic regression method was used to analyze the high-risk factors of premature birth, cesarean section, amniotic fluid aspiration, and asphyxia. The results showed that these factors were the risk factors of ARDS, as shown in Figure 10.

4. Discussion

Studies have shown that external infection and shock are common causes of ARDS [12, 13]. The pathogenesis of ARDS is not very clear, but clinical studies have shown that it is caused by lung and capillary injury. Lung damage, such as direct inhalation of venom, can cause systemic

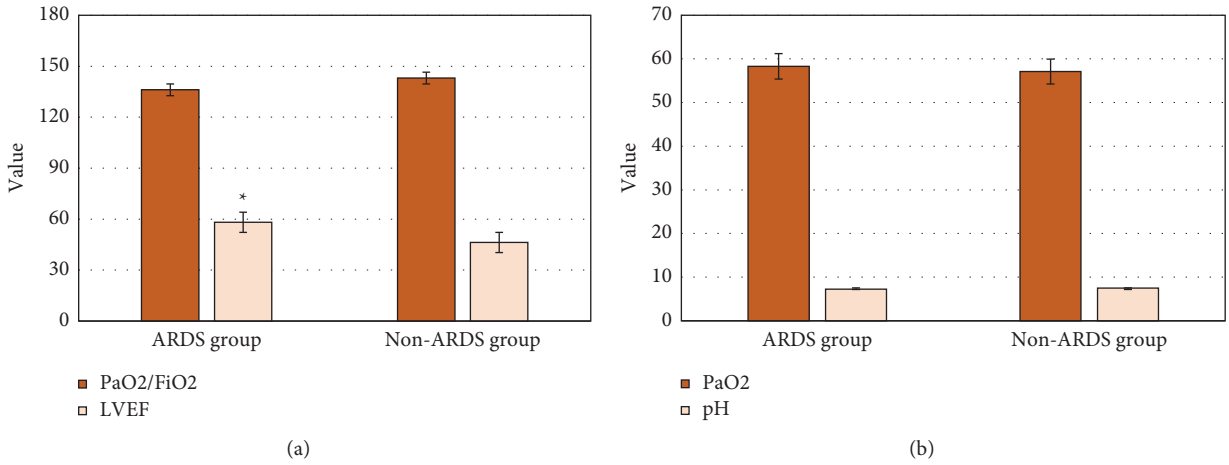

Figure 8: (a) Comparison of LVEF and P/F. (*The difference was statistically significant). (b) Comparison of pH and PaO_2. (*The difference was statistically significant).

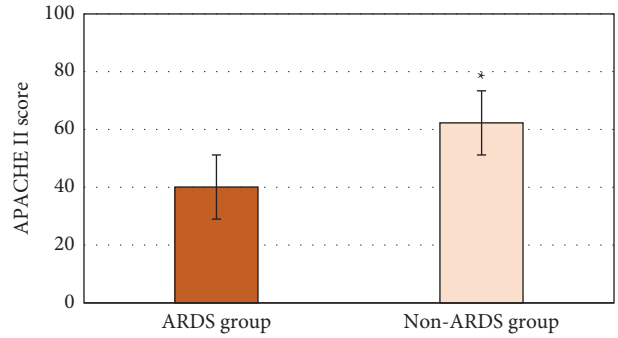

Figure 9: APACHE II scores in the two groups. (*The difference was statistically significant).

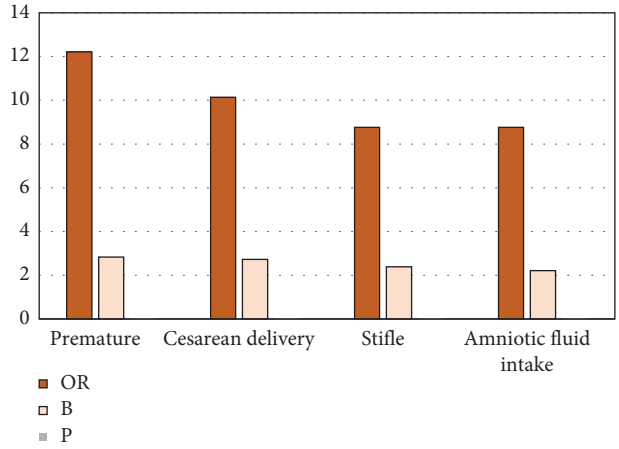

Figure 10: Analysis of related factors of ARDS.

inflammation, which increases the risk of ARDS [14, 15]. The most direct cause of ARDS is the migration and accumulation of inflammatory cells. The trauma and infection arise from the accumulation of endotoxin lipopolysaccharide in the capillaries of the lungs, causing acute respiratory diseases [16, 17]. Luyt et al. [18] stated in the article that one of the main complications of ARDS patients is pulmonary infection. In addition to traditional factors, pulmonary immune defense and imbalance of the microbiota are also pathogenic factors in ARDS patients. Matthay et al. [19] believed that ARDS is heterogeneous in clinical risk factors, lung injury physiology, microbiology, and biology and that identifying the phenotype of ARDS can strengthen the therapeutic effects. In this study, it was found that premature delivery, cesarean section, amniotic fluid aspiration, and asphyxia are the high-risk factors of ARDS.

Many algorithms are incorporated into CT imaging, such as deep learning, neural networks, and iterative reconstruction algorithms. They not only increase the scanning speed but also shorten the time of one rotation to 0.5 s. At the same time, multilayer images can be obtained. Because it is a fast volume scan, uninterrupted data collection can be performed on a large area of the body in a short time and the information obtained can also be increased [20]. The processed image has higher quality. The virtual endoscopy can improve the detection rate of small lesions and mucosal lesions. Introducing algorithms into CT imaging can effectively improve image quality. To maximize the quality of the image, algorithms and various noise reduction techniques are used to smooth the image. Hadia et al. [21] used the association classification algorithm to classify images, and confidence and support were used as evaluation criteria. It was found that the algorithm had good classification accuracy. In this study, the FWAC algorithm was used to process the CT images, in order to assist physicians in predicting ARDS. The results showed that the accuracy was 98.7%, which was significantly higher than that of the conventional CT imaging ($P < 0.05$).

5. Conclusion

To explore pathogenic factors of ARDS, in this study, the FWAC algorithm was used to process CT images. The results showed that the accuracy of the algorithm was as high as 98.7%. CT can reflect the severity of ARDS to a certain extent. CT imaging based on classification association algorithm is a reliable diagnostic method to ensure image quality and accurate diagnosis. The rules generated by FWAC were more accurate, assisting doctors in the prevention and diagnosis of ARDS disease. It was concluded that premature delivery and asphyxia are all high-risk factors of ARDS. However, some limitations in the study should be noted. The sample size is small, which will reduce the power of the study. In the follow-up study, expanded sample size is necessary to strengthen the findings of the study.

Data Availability

The data used to support the findings of this study are available from the corresponding author upon request.

Conflicts of Interest

The authors declare no conflicts of interest.

References

[1] E. L. Scholten, J. R. Beitler, G. K. Prisk, and A. Malhotra, "Treatment of ARDS with prone positioning," *Chest*, vol. 151, no. 1, pp. 215–224, 2017.

[2] T. J. Peck and K. A. Hibbert, "Recent advances in the understanding and management of ARDS," *F1000Res*, vol. 8, Article ID F1000, 2019.

[3] X. Li and X. Ma, "Acute respiratory failure in COVID-19: is it "typical" ARDS?" *Critical Care*, vol. 24, no. 1, p. 198, 2020.

[4] S. Metwaly, A. Cote, S. J. Donnelly, M. M. Banoei, A. I. Mourad, and B. W. Winston, "Evolution of ARDS biomarkers: will metabolomics be the answer?" *American Journal of Physiology - Lung Cellular and Molecular Physiology*, vol. 315, no. 4, pp. L526–L534, 2018.

[5] T. Pham and G. D. Rubenfeld, "Fifty years of research inARDS the epidemiology of acute respiratory distress syndrome. a 50th br," *American Journal of Respiratory and Critical Care Medicine*, vol. 195, no. 7, pp. 860–870, 2017.

[6] H. Yadav, B. T. Thompson, and O. Gajic, "Fifty years of research in ARDS is acute respiratory distress syndrome a preventable disease?" *American Journal of Respiratory and Critical Care Medicine*, vol. 195, no. 6, pp. 725–736, 2017.

[7] F. R. D'Alessio, "Mouse models of acute lung injury and ARDS," *Methods in Molecular Biology*, vol. 1809, pp. 341–350, 2018.

[8] R. Dembinski and F. Mielck, "Ards - an update - part 1: epidemiology, pathophysiology and diagnosis," *Anasthesiol Intensivmed Notfallmed Schmerzther*, vol. 53, no. 2, pp. 102–111, 2018.

[9] L. D. Bos, I. Martin-Loeches, and M. J. Schultz, "ARDS: challenges in patient care and frontiers in research," *European Respiratory Review*, vol. 27, no. 147, Article ID 170107, 2018.

[10] A. Pryor, Y. Yang, A. Rana et al., "GENFIRE: a generalized fourier iterative reconstruction algorithm for high-resolution 3D imaging," *Scientific Reports*, vol. 7, no. 1, Article ID 10409, 2017.

[11] K. Ito, K. Takumi, S. K. Meibom et al., "Risk assessment of osteoradionecrosis associated with periodontitis using 18F-FDG PET/CT," *European Journal of Radiology*, vol. 132, Article ID 109259, 2020.

[12] A. Gordon, E. Rabold, R. Thirumala, A. A. Husain, S. Patel, and T. Cheema, "Prone positioning in ARDS," *Critical Care Nursing Quarterly*, vol. 42, no. 4, pp. 371–375, 2019.

[13] J. G. Wilson and C. S. Calfee, "ARDS subphenotypes: understanding a heterogeneous syndrome," *Critical Care*, vol. 24, no. 1, p. 102, 2020.

[14] M. Umbrello, P. Formenti, L. Bolgiaghi, and D. Chiumello, "Current concepts of ARDS: a narrative review," *International Journal of Molecular Sciences*, vol. 18, no. 1, p. 64, 2016.

[15] G. Bellani, T. Pham, and J. G. Laffey, "Missed or delayed diagnosis of ARDS: a common and serious problem," *Intensive Care Medicine*, vol. 46, no. 6, pp. 1180–1183, 2020.

[16] B. A. McNicholas, G. M. Rooney, and J. G. Laffey, "Lessons to learn from epidemiologic studies in ARDS," *Current Opinion in Critical Care*, vol. 24, no. 1, pp. 41–48, 2018.

[17] T. Mauri, M. Lazzeri, G. Bellani, A. Zanella, and G. Grasselli, "Respiratory mechanics to understand ARDS and guide mechanical ventilation," *Physiological Measurement*, vol. 38, no. 12, pp. R280–H303, 2017.

[18] C.-E. Luyt, L. Bouadma, A. C. Morris et al., "Pulmonary infections complicating ARDS," *Intensive Care Medicine*, vol. 46, no. 12, pp. 2168–2183, 2020.

[19] M. A. Matthay, Y. M. Arabi, E. R. Siegel et al., "Phenotypes and personalized medicine in the acute respiratory distress syndrome," *Intensive Care Medicine*, vol. 46, no. 12, pp. 2136–2152, 2020.

[20] P. L. Silva, P. Pelosi, and P. R. M. Rocco, "Personalized pharmacological therapy for ARDS: a light at the end of the tunnel," *Expert Opinion on Investigational Drugs*, vol. 29, no. 1, pp. 49–61, 2020.

[21] W. E. Hadi, F. Aburub, and S. Alhawari, "A new fast associative classification algorithm for detecting phishing websites," *Applied Soft Computing*, vol. 48, pp. 729–734, 2016.